

# Shell Models for Magnetohydrodynamic Turbulence

Paolo Giuliani

Department of Physics, University of Calabria, 87036 Rende (CS), Italy

**Abstract.** We review the main properties of shell models for magnetohydrodynamic (MHD) turbulence. After a brief account on shell models with nearest neighbour interactions, the paper focuses on the most recent results concerning dynamical properties and intermittency of a model which is a generalization to MHD of the Gledzer-Yamada-Okhitani (GOY) model for hydrodynamic. Applications to astrophysical problems are also discussed.

## 1 Introduction

Shell models are dynamical systems (ordinary differential equations) representing a simplified version of the spectral Navier–Stokes or MHD equations for turbulence. They were originally introduced and developed by Obukhov [1], Desnyansky and Novikov [2] and Gledzer [3] in hydrodynamic turbulence and constitute nowadays a consistent and relevant alternative approach to the analytical and numerical study of fully developed turbulence (see [4] for a complete review).

Shell models are built up by dividing wave-vector space (k-space) in a discrete number of shells whose radii grow exponentially like  $k_n = k_0 \lambda^n$ , ( $\lambda > 1$ ),  $n = 1, 2, \dots, N$ . Each shell is assigned a scalar dynamic variable,  $u_n(t)$ , (real or complex) which takes into account the averaged effects of velocity modes between  $k_n$  and  $k_{n+1}$ . The equation for  $u_n(t)$  is then written in the form

$$\frac{du_n}{dt} = k_n C_n + D_n + F_n \quad (1)$$

where  $k_n C_n$ ,  $D_n$  and  $F_n$  are respectively quadratic nonlinear coupling terms (involving nearest or next-nearest shell interactions), dissipation terms and forcing terms, the last generally restricted to the first shells. Nonlinear terms are chosen to satisfy scale-invariance and conservation of ideal invariants. The main advantage shell models offer is that they can be investigated by means of rather easy numerical simulations at very high Reynolds ( $Re$ ) numbers. The degrees of freedom of a shell model are  $N \sim \ln Re$ , to be compared with  $N \sim Re^{9/4}$  for a three dimensional hydrodynamic turbulence following the Kolmogorov scaling.

The paper is organized as follows. In section 2 shell models with nearest neighbour interactions are briefly reviewed. In section 3 equations for MHD models with nearest and next-nearest neighbour interactions are presented

and conservations laws for the ideal case are discussed. Section 4 is devoted to dynamo action in shell models and section 5 to spectral properties in forced stationary state and intermittency. In section 6 conclusions are drawn and a brief mention to astrophysical applications is made.

## 2 Models with nearest neighbour interactions

The simplest hydrodynamic shell model is the Obukhov–Novikov model, which is a linear superposition of the Obukhov equation [1] and the Novikov equation [2]. The model involves real variables  $u_n(t)$  and conserves the energy  $1/2 \sum_{n=1}^N u_n^2$  in absence of forcing and dissipation. It does not conserve phase space volume nor other quadratic invariants exist. The extension of the Obukhov–Novikov model to MHD is due to Gloaguen *et al.* [5]. We write down the equations for clarity ( $u_n$  and  $b_n$  represent respectively the velocity and the magnetic field in dimensionless units)

$$\begin{aligned} \frac{du_n}{dt} &= -\nu k_n^2 u_n + \alpha (k_n u_{n-1}^2 - k_{n+1} u_n u_{n+1} - k_n b_{n-1}^2 + k_{n+1} b_n b_{n+1}) \\ &\quad + \beta (k_n u_{n-1} u_n - k_{n+1} u_{n+1}^2 - k_n b_n b_{n-1} + k_{n+1} b_{n+1}^2) \\ \frac{db_n}{dt} &= -\eta k_n^2 b_n + \alpha k_{n+1} (u_{n+1} b_n - u_n b_{n+1}) + \beta k_n (u_n b_{n-1} - u_{n-1} b_n) \end{aligned} \quad (2)$$

$$\frac{db_n}{dt} = -\eta k_n^2 b_n + \alpha k_{n+1} (u_{n+1} b_n - u_n b_{n+1}) + \beta k_n (u_n b_{n-1} - u_{n-1} b_n) \quad (3)$$

Here  $\nu$  is the kinematic viscosity,  $\eta$  is the magnetic diffusivity,  $\alpha$  and  $\beta$  are two arbitrary coupling coefficients. The ideal invariants of the system are the total energy,  $1/2 \sum_{n=1}^N (u_n^2 + b_n^2)$  and the cross-correlation,  $\sum_{n=1}^N u_n b_n$  which are two ideal invariants of the MHD equations [6]. When written in terms of the Elsässer variables  $Z_n^+ = u_n + b_n$ ,  $Z_n^- = u_n - b_n$ , the equations assume a symmetric form and the conservation of the two previous invariants is equivalently expressed as the conservation of the pseudo-energies  $E^\pm = (1/4) \sum_{n=1}^N Z_n^\pm{}^2$ . It is remarkable to note that, unlike the hydrodynamic model, the MHD version satisfies a Liouville theorem  $\sum_{n=1}^N \partial(dZ_n^\pm/dt)/\partial Z_n^\pm = 0$ , implying phase-space volume conservation. The MHD equations conserve a third ideal invariant which is the magnetic helicity in three dimensions (3D) and the mean square potential in two dimensions (2D), but no further ideal quadratic invariant can be imposed to this shell model.

A detailed bifurcation analysis for a three-mode system was performed in [5] for different values of  $\alpha$  and  $\beta$ . The low Reynolds (kinetic and magnetic) numbers, used as control parameters, allowed to identify a great variety of regions in the parameter space. Turbulence was investigated with a nine-mode system which produces an inertial range with spectra following approximately the Kolmogorov scaling  $E(k) \sim k^{-5/3}$ . Temporal intermittency was also observed and then reconsidered in more details by Carbone [7] who calculated the scaling exponents of the structure functions for the Elsässer variables and for the pseudo-energy transfer rates, showing consistency with the usual

multifractal theory. Other interesting MHD phenomena were also observed in [5] such as dynamo effect and the growth of correlation between velocity and magnetic field in an unforced simulation. These phenomena will be treated in more details in the next paragraphs.

The complex version of (2) and (3) was thoroughly investigated by Biskamp [8]. The complex model allows to include the Alfvén effect [9], [10], [11], that is the interaction of a constant large scale magnetic field with small scale turbulent eddies. The main consequence of this effect should be a reduction of the spectral energy transfer rate and a consequent change of the spectra from the Kolmogorov scaling,  $E(k) \sim k^{-5/3}$ , to the Iroshnikov-Kraichnan one,  $E(k) \sim k^{-3/2}$ . In this paper the Alfvén effect will not be furtherly treated. The reader is referred to [8] for a complete discussion concerning the inclusion of Alfvénic terms in shell models.

### 3 Models with nearest and next-nearest interactions

Shell models with nearest and next-nearest neighbour interactions were introduced by Gledzer [3]. In particular the so called GOY (Gledzer-Yamada-Ohkitani) model has been extensively both numerically and analytically investigated [12], [13], [14]. The GOY model allows to conserve another quadratic invariant besides energy which was identified with the kinetic helicity [15]. A generalization of the GOY model to MHD can be found in Biskamp [8]. All the parameters of the model are now fixed by imposing the conservation of another quadratic invariant that can be chosen to distinguish between a 3D and a 2D model. A more refined version was then considered by Frick and Sokoloff [16] to take into account the fact that the magnetic helicity is a quantity not positive definite. The situation can be summarized as follows [17].

Let us consider the following set of equations ( $u_n$  and  $b_n$  are now complex variables representing the velocity and the magnetic field in dimensionless units)

$$\begin{aligned} \frac{du_n}{dt} = & -\nu k_n^2 u_n - \nu' k_n^{-2} u_n + ik_n \left\{ (u_{n+1} u_{n+2} - b_{n+1} b_{n+2}) \right. \\ & \left. - \frac{\delta}{\lambda} (u_{n-1} u_{n+1} - b_{n-1} b_{n+1}) - \frac{1-\delta}{\lambda^2} (u_{n-2} u_{n-1} - b_{n-2} b_{n-1}) \right\}^* + f_n \quad (4) \end{aligned}$$

$$\begin{aligned} \frac{db_n}{dt} = & -\eta k_n^2 b_n + ik_n \left\{ (1-\delta-\delta_m) (u_{n+1} b_{n+2} - b_{n+1} u_{n+2}) \right. \\ & \left. + \frac{\delta_m}{\lambda} (u_{n-1} b_{n+1} - b_{n-1} u_{n+1}) + \frac{1-\delta_m}{\lambda^2} (u_{n-2} b_{n-1} - b_{n-2} u_{n-1}) \right\}^* + g_n \quad (5) \end{aligned}$$

or, in terms of the complex Elsässer variables  $Z_n^\pm(t) = v_n(t) \pm b_n(t)$ , particularly useful in some solar-wind applications,

$$\frac{dZ_n^\pm}{dt} = -\nu^+ k_n^2 Z_n^\pm - \nu^- k_n^2 Z_n^\mp - \frac{\nu'}{2} k_n^{-2} Z_n^+ - \frac{\nu'}{2} k_n^{-2} Z_n^- + ik_n T_n^{\pm*} + f_n^\pm \quad (6)$$

where

$$T_n^\pm = \left\{ \begin{aligned} & \frac{\delta + \delta_m}{2} Z_{n+1}^\pm Z_{n+2}^\mp + \frac{2 - \delta - \delta_m}{2} Z_{n+1}^\mp Z_{n+2}^\pm \\ & + \frac{\delta_m - \delta}{2\lambda} Z_{n+1}^\pm Z_{n-1}^\mp - \frac{\delta + \delta_m}{2\lambda} Z_{n+1}^\mp Z_{n-1}^\pm \\ & - \frac{\delta_m - \delta}{2\lambda^2} Z_{n-1}^\pm Z_{n-2}^\mp - \frac{2 - \delta - \delta_m}{2\lambda^2} Z_{n-1}^\mp Z_{n-2}^\pm \end{aligned} \right\} \quad (7)$$

Here  $\nu^\pm = (\nu \pm \eta)/2$ , being  $\nu$  the kinematic viscosity and  $\eta$  the resistivity,  $-\nu' k_n^{-2} u_n$ , eq. (4), is a drag term specific to 2D cases (see below),  $f_n^\pm = (f_n \pm g_n)/2$  are external driving forces,  $\delta$  and  $\delta_m$  are real coupling coefficients to be determined. In the inviscid unforced limit, equations (6) conserve both pseudoenergies  $E^\pm(t) = (1/4) \sum_n |Z_n^\pm(t)|^2$  for any value of  $\delta$  and  $\delta_m$  (the sum is extended to all the shells), which corresponds to the conservation of both the total energy  $E = E^+ + E^- = (1/2) \sum_n (|v_n(t)|^2 + |b_n(t)|^2)$  and the cross-helicity  $h_C = E^+ - E^- = \sum_n \text{Re}(v_n b_n^*)$ . As far as the third ideal invariant is concerned, we can define a generalized quantity as

$$H_B^{(\alpha)}(t) = \sum_{n=1}^N (\text{sign}(\delta - 1))^n \frac{|b_n(t)|^2}{k_n^\alpha} \quad (8)$$

whose conservation implies  $\delta = 1 - \lambda^{-\alpha}$ ,  $\delta_m = \lambda^{-\alpha}/(1 + \lambda^{-\alpha})$  for  $\delta < 1$ ,  $0 < \delta_m < 1$  and  $\delta = 1 + \lambda^{-\alpha}$ ,  $\delta_m = -\lambda^{-\alpha}/(1 - \lambda^{-\alpha})$  for  $\delta > 1$ ,  $\delta_m < 0$ ,  $\delta_m > 1$ . Thus two classes of MHD GOY models can be defined with respect to the values of  $\delta$ : 3D-like models for  $\delta < 1$ , where  $H_B^{(\alpha)}$  is not positive definite and represents a generalized magnetic helicity; 2D-like models where  $\delta > 1$  and  $H_B^{(\alpha)}$  is positive definite. This situation strongly resembles what happens in the hydrodynamic case where 2D-like ( $\delta > 1$ ) and 3D-like ( $\delta < 1$ ) models are conventionally distinguished with respect to a second generalized conserved quantity  $H_K^{(\alpha)}(t) = \sum_n (\text{sign}(\delta - 1))^n k_n^\alpha |v_n(t)|^2$ . Here the 3D and 2D cases are recovered for  $\alpha = 1, 2$  where the ideal invariants are identified respectively with kinetic helicity and enstrophy. It should be noted that, although the hydrodynamic invariants are not conserved in the magnetic case, the equations which link  $\alpha$  and  $\delta$  are exactly the same for hydrodynamic and MHD models. Thus, once fixed  $\alpha$  and  $\delta$ , it is a simple matter to find out which GOY model the MHD GOY one reduces to when  $b_n = 0$  [17]. To summarize we have that (with  $\lambda = 2$ ) the model introduced in [16] for the 3D case will be called, hence on, 3D MHD GOY model or simply 3D model. It is recovered for  $\alpha = 1$ ,  $\delta = 1/2$ ,  $\delta_m = 1/3$  and reduces to the usual 3D GOY model for  $b_n = 0$ . The Biskamp's 3D model [8] is actually a 2D-like model and will be called pseudo 3D model. It is obtained for  $\alpha = 1$ ,  $\delta = 3/2$ ,  $\delta_m = -1$  and reduces to a 2D-like GOY model that conserves a quantity which has the same dimensions as kinetic helicity but is positive definite. The 2D models introduced in [8] and in [16] coincide, they are recovered for  $\alpha = 2$ ,  $\delta = 5/4$ ,

$\delta_m = -1/3$  and reduce to the usual 2D GOY model for  $b_n = 0$ . In the following the properties of the 3D model will be mainly investigated.

## 4 Dynamo action in MHD shell models

The problem of magnetic dynamo, that is the amplification of a seed of magnetic field and its maintenance against the losses of dissipation in an electrically conducting flow, is of great interest by itself and for astrophysical applications (see for example [18] for an excellent introduction to the problem). Shell models offer the opportunity to test with relative simplicity whether a small value of the magnetic field can grow in absence of forcing terms on the magnetic field. Previous considerations about dynamo action in shell models can be found in [5]. In that case numerical study of bifurcations in the three-mode system revealed instabilities of kinetic fixed points to magnetic ones or magnetic chaos. The existence of a sort of dynamo effect in MHD GOY models was put forward by Frick and Sokoloff [16]. The authors investigate the problem of the magnetic field generation in a free-decaying turbulence, thus showing that: 1) in the 3D case magnetic energy grows and reaches a value comparable with the kinetic one, in a way that the magnetic field growth is unbounded in the kinematic case; 2) in the 2D case magnetic energy slowly decays in the nonlinear as well as in the kinematic case. These results have been interpreted as a 3D “turbulent dynamo effect” and seem to be in agreement with well-known results by which dynamo effect is not possible in two dimensions [19]. The problem was then reexamined in [17] in a forced situation looking at a comparison between the 3D MHD GOY model and the pseudo 3D model.

Starting from a well developed turbulent velocity field, a seed of magnetic field is injected and the growth of the magnetic spectra monitored. System is forced on the shell  $n = 4$  ( $k_0 = 1$ ), setting  $f_4^+ = f_4^- = (1 + i) 10^{-3}$ , which corresponds to only inject kinetic energy at large scales. Method of integration is a modified fourth order Runge-Kutta scheme. In fig. 1 we plot  $\log_{10} \langle |b_n|^2 \rangle$  and  $\log_{10} \langle |v_n|^2 \rangle$  versus  $\log_{10} k_n$  for the 3D model. Angular brackets  $\langle \rangle$  stand for time averages. It can be seen that the magnetic energy grows rapidly in time and forms a spectrum where the amplitude of the various modes is, at small scale, of the same order as the kinetic energy spectrum. (The subsequent evolution of magnetic and kinetic spectra will be considered in the next section). The spectral index is close to  $k^{-2/3}$  which is compatible with a Kolmogorov scaling of the second order structure function. For a comparison we integrated the pseudo 3D model and it can be seen (fig. 2) that a magnetic spectrum is formed, but it slowly decays in time. Notice that, because of the smallness of  $b_n$ , its back-reaction on the velocity field is negligible, thus the kinematic part of the model evolves independently from the magnetic one. Now the scaling  $|v_n|^2 \sim k_n^{-4/3}$  follows, as a cascade of generalized enstrophy

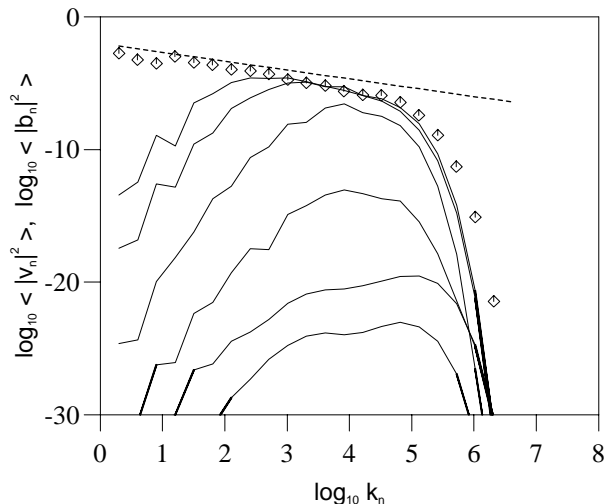


**Fig. 1.** 3D model:  $\log_{10}\langle |v_n|^2 \rangle$  (*diamonds*) and  $\log_{10}\langle |b_n|^2 \rangle$  (*lines*) versus  $\log_{10} k_n$ . The averages of  $|b_n|^2$  are made over intervals of 3 large scale turnover times. Time proceeds upwards. The kinetic spectrum is averaged over 30 large scale turnover times. The straight line has slope  $-2/3$ . Parameters used:  $N=24$ ,  $\nu = \eta = 10^{-8}$ ,  $\nu' = 0$

is expected for 2D-like hydrodynamic GOY models when  $\alpha < 2$  (see [20] for details). The question now arises whether it is correct the interpretation of the growth of the magnetic field in the 3D model as the corresponding dynamo effect expected in the real 3D magnetohydrodynamics. First of all it should be noted that in the kinematic case an analogy with the vorticity equation predicts the following relations between velocity and magnetic energy spectra [6]:  $|v_n|^2 \sim k^{-a}$ ,  $|b_n|^2 \sim k^{2-a}$ , so that if  $a = 2/3$  it follows a magnetic energy spectrum growing with  $k$ . The kinematic case corresponds to the first stage of growth of our simulation where this behaviour is sometimes visible, at least qualitatively. Note however that the averages are made on very small time intervals because of the rapid growth of the magnetic energy. A similar, much more pronounced behaviour is found for the pseudo 3D model as well.

Let us stress that the sign of the third ideal invariant seems to play a crucial role as far as the growth of small magnetic fields is concerned. In effect this sort of dynamo effect can also be considered under a different point of view. Let us consider the ideal evolution of the model  $dZ_n^\pm/dt = ik_n T_n^{\pm*}$ . We can build up the phase space  $S$  of dimension  $D = 4N$ , by using the Elsässer variables as axes, so that a point in  $S$  represents the system at a given time. A careful analysis of (6) shows that there exist some subspaces  $I \subset S$  of dimension  $D = 2N$  which remain invariant under the time evolution [21]. More formally, let  $y(0) = (v_n, b_n)$  be a set of initial conditions such that  $y(0) \in I$ ,  $I$  is time invariant if the flow  $T^t$ , representing the time

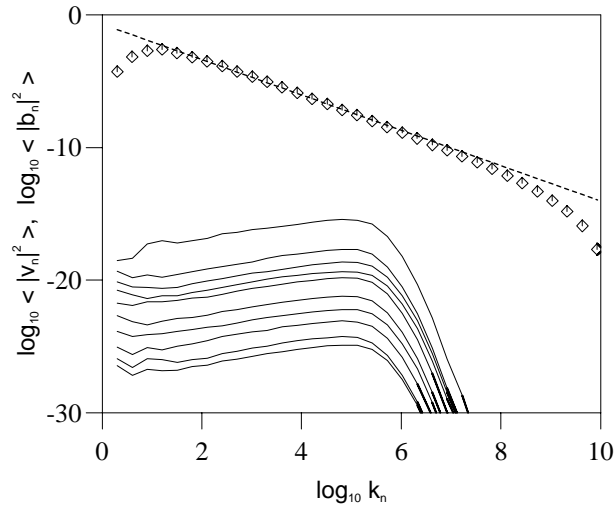


**Fig. 2.** Pseudo 3D model:  $\log_{10}\langle |v_n|^2 \rangle$  (diamonds) and  $\log_{10}\langle |b_n|^2 \rangle$  (lines) versus  $\log_{10} k_n$ . Averages are made over intervals of 100 large scale turnover times. Time proceeds downwards. The kinetic spectrum is only shown for the last interval. The straight line has slope  $-4/3$ , see text for explanation. Parameters used:  $N=33$ ,  $\nu = 10^{-16}$ ,  $\eta = 0.5 \cdot 10^{-9}$ ,  $\nu' = 1$

evolution operator in  $S$ , leaves  $I$  invariant, that is  $T^t[y(0)] = y(t) \in I$ . The kinetic subspace  $K \subset S$ , defined by  $y(0) = (v_n, 0)$  is obviously the usual fluid GOY model. Further subspaces are the Alfvénic subspaces  $A^\pm$  defined by  $y(0) = (v_n, \pm v_n)$ , say  $Z_n^+ \neq 0$  and  $Z_n^- = 0$  (or vice versa). Each initial condition in these subspaces is actually a fixed point of the system. We studied the properties of stability of  $K$  and  $A^\pm$ . Following [21], let us define for each  $I$  the orthogonal complement  $P$ , namely  $S = I \oplus P$ . Let us then decompose the solution as  $y(t) = (y_{int}(t), y_{ext}(t))$  where the subscripts refer to the  $I$  and  $P$  subspaces respectively. Finally we can define the energies  $E_{int} = \|y_{int}\|^2$  and  $E_{ext} = \|y_{ext}\|^2$ . Note that the distance of a point  $y = (y_{int}, y_{ext})$  from the subspace  $I$  is  $d = \min_{\hat{y} \in I} \|y - \hat{y}\| = \|y_{ext}\|$ . Then  $E_{ext}$  represents the square of the distance of the solution from the invariant subspace. At time  $t = 0$ ,  $E_{ext} = \epsilon E_{int}$  ( $\epsilon \ll 1$ ) represents the energy of the perturbation. Since the total energy is constant in the ideal case, two extreme situations can arise: 1) The external energy remains of the same order of its initial value, that is the solution is trapped near  $I$  which is then a stable subspace; 2) The external energy assumes values of the same order as the internal energy, that is the solution is repelled away from the subspace which is then unstable. Since the external and internal energies for the Alfvénic subspaces are nothing but the pseudoenergies  $E^+$  and  $E^-$ , which are ideal invariants, the Alfvénic subspaces are stable. As regards the kinetic subspace,  $E_{int}$  and  $E_{ext}$  represent respectively the kinetic and magnetic energies. Looking at the numerical solutions

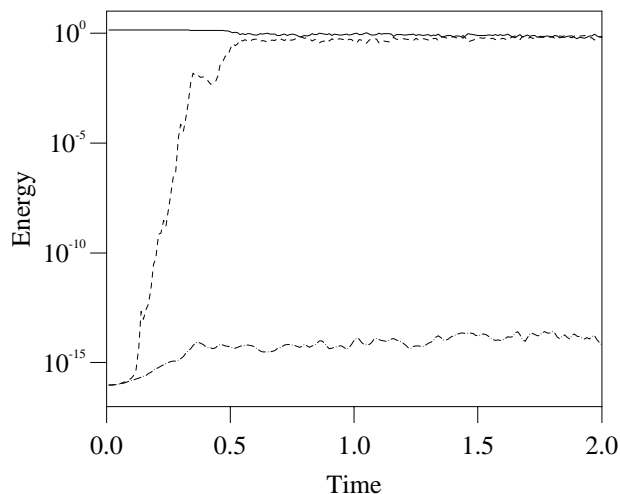


**Fig. 3.** Ideal case: kinetic energy (*continuous line*) and magnetic energy (*dashed line*) versus time for the 3D model; magnetic energy (*dot-dashed line*) versus time for the pseudo 3D model

of the ideal model (fig. 3) we can see the difference in the stability properties between the pseudo 3D model and the 3D one. In the first case the external energy remains approximately constant, while in the second case the system fills up immediately all the available phase space. This striking difference is entirely due to the nonlinear term, and in fact must be ascribed to the differences in sign of the third invariant. The effect of the unstable subspace, which pushes away the solutions, is what in ref. [16] is called “turbulent dynamo effect”.

## 5 Spectral properties in stationary forced state

The main fundamental difference between hydrodynamic and MHD shell models lies in the fact that the behaviour of the former is not so sensitive to the type of forcing, at least as far as the main features are concerned. On the contrary in the magnetic case phase space is more complex because of the presence of invariant subspaces which can act as attractors of the dynamics of the system, hence the type of forcing becomes crucial in selecting the stationary state reached by the system. The spectral properties of the 3D model have been investigated by Frick and Sokolov in [16] under different choices of the forcing terms. In their simulations they observe that the spectral indexes of kinetic and magnetic spectra depend on the level of cross helicity and magnetic helicity. In particular spectra with spectral index  $-5/3$  appear if the cross helicity vanishes. Even in this case results may be deceptive. In fact, defining the reduced cross helicity  $h_R$  as the cross helicity divided by

the total energy, long runs [17] show that, in case of constant forcing on the velocity variables, even from an initial value  $h_R = 0$  the system evolves inevitably towards a state in which the reduced cross helicity reaches either the value +1 or -1, corresponding to a complete correlation or anti-correlation between velocity and magnetic field. In terms of attractors the system is attracted towards one of the Alfvénic subspaces where velocity and magnetic field are completely aligned or anti-aligned. Due to the particular form of the nonlinear interactions in MHD (6), the nonlinear transfer of energy towards the small scales is stopped. In this case Kolmogorov-like spectra appear as a transient of the global evolution. This is shown in fig.4 where it is clearly seen a component ( $Z_n^-$ ) which is completely vanishing while the  $Z_n^+$  spectrum becomes steeper and steeper as energy is not removed from large scales. If an exponentially correlated in time gaussian random forcing on the velocity field is adopted the system shows a very interesting behaviour. It spends long periods (several large scale turnover times) around one of the Alfvénic attractors, jumping from one to the other rather irregularly (fig. 5). This behaviour assures the existence of a flux of energy to the small scales, modulates the level of nonlinear interactions and the consequent dissipation of energy at small scales, which is burstly distributed in time. What we want to stress is the fact that the Alfvénic attractors play a relevant role in the dynamics of the system. This fact should be taken into account especially when a stationary state is investigated in order to determine the scaling exponents of the structure functions (see below). Two regimes, the Kolmogorov transient and the completely aligned regime, could be mixed during the average procedure, thus leading to unreliable values of the scaling exponents.

## 6 Fluxes, Inertial Range and Intermittency

The “four-fifth” relation  $\langle \delta v(l)^3 \rangle = (-4/5)\epsilon l$ , where  $\epsilon$  is the mean rate of energy dissipation and  $l$  the separation, derived by Kolmogorov in [22], can be generalized to MHD flows [23],[24],[25]. A corresponding relation exists in MHD shell models, which can be derived following the considerations in [26]. Assuming for simplicity  $\nu = \eta$ , the scale-by-scale energy budget equation is:

$$\frac{d}{dt} \sum_{i=1,n} \frac{|Z_i^\pm|^2}{4} = k_n (Z^\pm Z^\pm Z^\mp)_n - \nu \sum_{i=1,n} k_i^2 \frac{|Z_i^\pm|^2}{2} + \sum_{i=1,n} \frac{1}{2} \text{Re}\{Z_i^\pm (f_i^\pm)^*\}$$

where the quantities  $(Z^\pm Z^\pm Z^\mp)_n$  are defined as

$$\begin{aligned} (Z^\pm Z^\pm Z^\mp)_n &= \frac{1}{4} \text{Im}\{(\delta + \delta_m)\} Z_n^\pm Z_{n+1}^\pm Z_{n+2}^\mp + \frac{(2 - \delta - \delta_m)}{\lambda} Z_{n-1}^\pm Z_n^\mp Z_{n+1}^\pm \\ &+ (2 - \delta - \delta_m) Z_n^\pm Z_{n+1}^\mp Z_{n+2}^\pm + \frac{(\delta_m - \delta)}{\lambda} Z_{n-1}^\mp Z_n^\pm Z_{n+1}^\pm \end{aligned} \quad (9)$$

Assuming that i) forcing terms only act at large scales; (ii) the system tends to a statistically stationary state; (iii) in the infinite Reynolds numbers limit

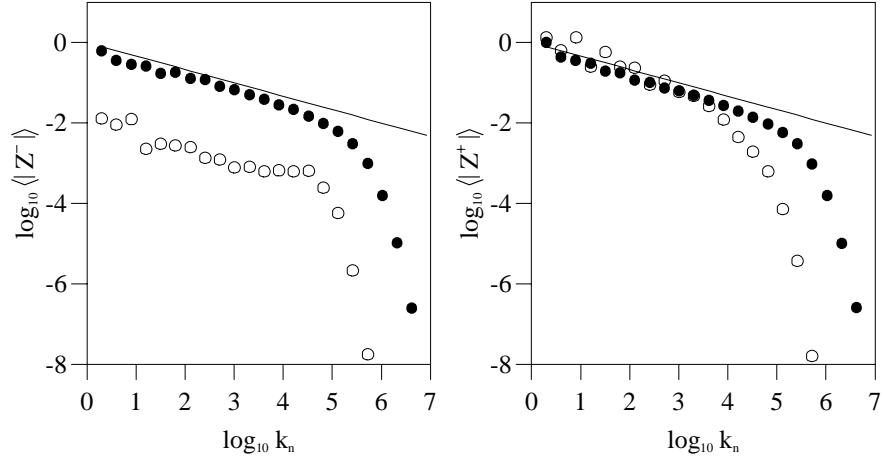


**Fig. 4.** *Left:*  $\log_{10}\langle |Z_n^-| \rangle$  versus  $\log_{10} k_n$  at different times (a) Black circles: The average of  $|Z_n^-|$  are made over the first 30 large scale turnover times (b) White circles: The average is made after 300 large scale turnover times (c). The straight line has slope  $-1/3$ . *Right:* The same for  $|Z_n^+|$

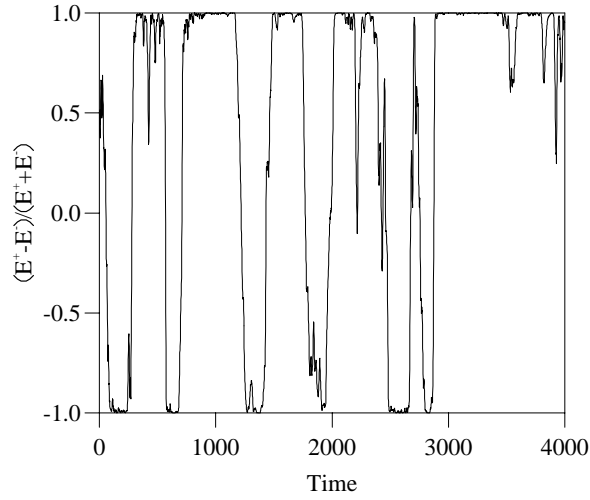


**Fig. 5.** Reduced cross helicity versus time in the case of an exponentially time-correlated random gaussian forcing on the velocity variables

( $\nu \rightarrow 0$ ) the mean energy dissipation tends to a finite positive limit  $\varepsilon^\pm$ , we obtain

$$\begin{aligned}\langle (Z^+ Z^+ Z^-)_n \rangle &= -\varepsilon^+ k_n^{-1} \\ \langle (Z^- Z^- Z^+)_n \rangle &= -\varepsilon^- k_n^{-1}\end{aligned}$$

These are the equations that define the inertial range of the system and that can be easily checked and confirmed by numerical simulations (fig. 6). It is to be remarked that these are the appropriate combinations that are expected to scale exactly as  $k^{-1}$ . Let us finally remind that, as far as cascade properties

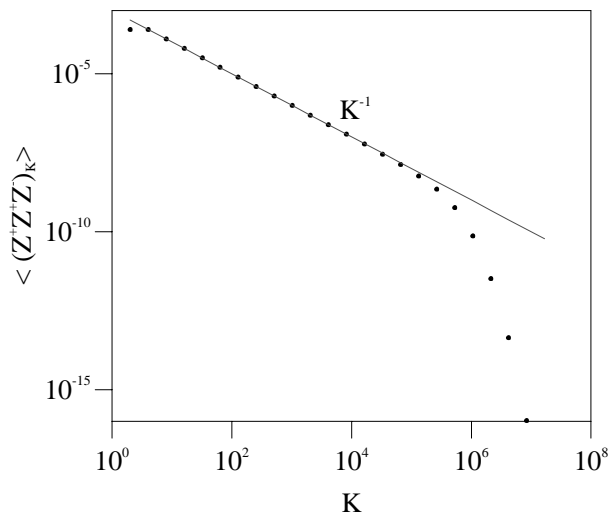


**Fig. 6.** Numerical check of the exact scaling relation involving the mixed third order moment

of shell models are concerned, the major drawback lies in the difficulty to reproduce cascades of quantities that are expected to flow inversely, such as energy in 2D hydrodynamic [20] or magnetic helicity in MHD [8].

A deep understanding of intermittency in turbulence is nowadays one of the most challenging tasks from a theoretical point of view (see [27] for review). A lot of papers have been dedicated in the last years to investigate temporal intermittency in shell models. Deviations from the Kolmogorov scaling  $\xi_p = p/3$  of the scaling exponents in the structure functions,  $\langle |u_n|^p \rangle \sim k^{-\xi_p}$ , have been observed and described in the context of a multifractal approach [13]. A precise calculation of the scaling exponents may have difficulties related to the presence of periodic oscillations superimposed to the power law. Another source of uncertainty is linked to the exact identification of the inertial range where the fit should be performed. These problems are at length discussed and investigated in [28] where a new shell model (called Sabra

model) has been introduced in the context of hydrodynamic turbulence. The Sabra model is a slight modification of the standard GOY model and allows to eliminate spurious oscillations in the spectra. The same problems are in principle encountered in magnetohydrodynamic models thus a generalization of the Sabra model to MHD is required ([29]). An alternative approach to the determination of scaling exponents for the 3D MHD GOY model can be found in [30] where concepts and techniques related to ESS and GESS [31] are used.

We have determined the scaling exponents of the structure functions  $\langle |u_n|^p \rangle \sim k^{-\xi_p^u}$ ,  $\langle |b_n|^p \rangle \sim k^{-\xi_p^b}$ ,  $\langle |Z_n^+|^p \rangle \sim k^{-\xi_p^+}$ ,  $\langle |Z_n^-|^p \rangle \sim k^{-\xi_p^-}$  adopting a random forcing on the velocity variables (on shell  $n=1$  and  $n=2$ ) to assure the system does not “align”. The forcing terms were calculated solving a Langevin equation  $\dot{f}_n = -(1/\tau_0) f_n + \mu$ , where  $\tau_0$  is a correlation time chosen equal to the large scale turnover time and  $\mu$  is a gaussian delta-correlated noise. The total number of shells is 23 and the values of viscosity and resistivity are  $\nu = 0.5 \cdot 10^{-9}$ ,  $\eta = 0.5 \cdot 10^{-9}$ . In fig. 7 the first three structure functions are plotted for the magnetic field, together with the best fit lines. From a comparison with spectra obtained in the standard GOY model [26], it should be remarked that the cross over region between the inertial range and the dissipative one is not so sharp as in the hydrodynamic case.

We then decided to perform a least-square fit in the range, determined visually, between the shell numbers  $n = 3$  and  $n = 12$ . The values of  $\xi_p^u$  and

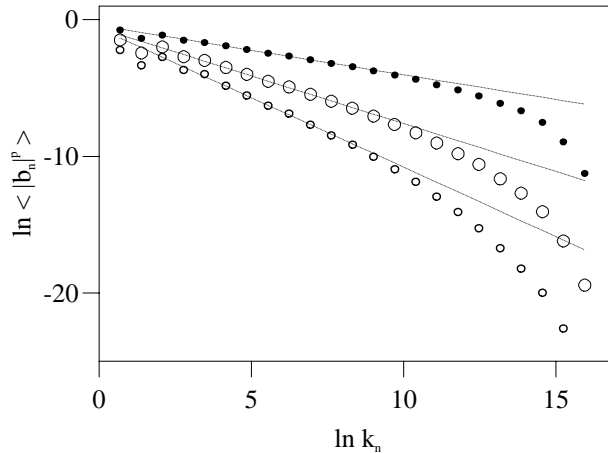


**Fig. 7.** Structure functions  $\ln\langle |b_n|^p \rangle$  versus  $\ln k_n$  for (a)  $p = 1$  (black circles) (b)  $p = 2$  (large white circles) (c)  $p = 3$  (small white circles). The straight lines are the best fit in the range between  $n = 3$  and  $n = 12$

$\xi_p^b$  are reported in Table 1 together with the values of  $\xi_p$ , extracted from [26], for the hydrodynamic GOY model. The values of the scaling exponents of the

other structure functions are compatible, within errors coming from the fit procedure, with those of the velocity variables. It can be seen that the values found are compatible with those obtained for the standard hydrodynamic GOY model.

**Table 1.** Scaling exponents  $\xi_p$  (GOY model),  $\xi_p^u$ ,  $\xi_p^b$

$p$	$\xi_p$ (GOY)	$\xi_p^u$	$\xi_p^b$
1		$0.37 \pm 0.01$	$0.36 \pm 0.01$
2	0.72	$0.71 \pm 0.01$	$0.70 \pm 0.01$
3	1.04	$1.02 \pm 0.02$	$1.02 \pm 0.02$
4	1.34	$1.31 \pm 0.03$	$1.32 \pm 0.03$
5	1.61	$1.57 \pm 0.04$	$1.59 \pm 0.04$
6	1.86	$1.82 \pm 0.05$	$1.84 \pm 0.05$
7	2.11	$2.05 \pm 0.06$	$2.07 \pm 0.06$
8	2.32	$2.28 \pm 0.08$	$2.30 \pm 0.08$

## 7 Conclusions

In this paper we have reported about the main properties concerning dynamical behaviour and intermittency of a shell model for MHD turbulence. The properties of the model reveal a complex structure of phase space in which invariant subspaces are present. The stability properties of the kinetic subspace are related to a dynamo action in the system while Alfvénic subspaces act as strong attractors which cause the system to evolve towards a state in which no energy cascade is present. A careful choice of forcing terms seems to be crucial in determining the stationary state reached by the system.

We want finally mention that shell models, as good candidates to reproduce the main features of MHD turbulence, can be used to check conjectures and ideas in astrophysical applications where very high Reynolds numbers are often present. We briefly remind two examples of applications. In [32] MHD shell models have been used to simulate magnetohydrodynamics in the early universe to investigate the effects of plasma viscosity on primordial magnetic fields. As second example, scaling laws found in the probability distribution functions of quantities connected with solar flares (eruption events in the solar corona) are at present matter of investigation by means of shell models. Results on this subject can be found in [33].

I am grateful to Vincenzo Carbone, Pierluigi Veltri, Leonardo Primavera, Guido Boffetta, Antonio Celani and Angelo Vulpiani for useful discussions and suggestions.

## References

1. Obukhov A. M., *Atmos. Oceanic Phys.*, **7** (1971) 41.
2. Desnyanski V. N. and Novikov E. A., *prik. Mat. Mekh.*, **38** (1974) 507.
3. Gledzer E. B., *Dokl. Akad. Nauk SSSR*, **208** (1973) 1046.
4. Bohr T., Jensen M. H., Paladin G. and Vulpiani A., *Dynamical Systems Approach to Turbulence* (Cambridge University Press) 1998.
5. Gloaguen C., Leorat J., Pouquet A. and Grappin R., *Physica D* **17** (1985) 154.
6. Biskamp D., *Nonlinear Magnetohydrodynamics* (Cambridge University Press) 1993.
7. Carbone V., *Europhys. Lett.*, **27** (1994) 581.
8. Biskamp D., *Phys. Rev. E*, **50** (1994) 2702; *Chaos, Solitons & Fractals*, **5** (1995) 1779.
9. Iroshnikov P. S., *Astron. Zh.*, **40** (1963) 742.
10. Kraichnan R. H., *Phys. Fluids*, **8** (1965) 1385.
11. Dobrowolny M., Mangeney A. and Veltri P., *Phys. Rev. Lett.*, **45** (1980) 1440.
12. Yamada M., Ohkitani K., *J. Phys. Soc. Jpn.*, **56** (1987) 4810.
13. Jensen M. H., Paladin G. and Vulpiani A., *Phys. Rev. A*, **43** (1991) 798.
14. Biferale L., Lambert A., Lima R. and Paladin G., *Physica D*, **80** (1995) 105.
15. Kadanoff L., Lohse D., Wang J. and Benzi R., *Phys. Fluids*, **7** 1995 617.
16. Frick P. and Sokoloff D. D., *Phys. Rev. E.*, **57** (1998) 4195.
17. Giuliani P. and Carbone V., *Europhys. Lett.*, **43** (1998) 527.
18. Moffat H. K., *Magnetic Field Generation in Electrical Conducting Fluids* (Cambridge University Press) 1978.
19. Zeldovich Ya. B., *Sov. Phys. JETP*, **4** (1957) 460.
20. Ditlevsen P. and Mogensen I. A., *Phys. Rev. E*, **53** (1996) 4785.
21. Carbone V. and Veltri P., *Astron. Astrophys.*, **259** (1992) 359.
22. Kolmogorov A. N., *Dokl. Akad. Nauk SSSR*, **32** (1941) 19.
23. Chandrasekhar S., *Proc. R. Soc. London, Ser. A* **204**, (1951) 435.
24. Chandrasekhar S., *Proc. R. Soc. London, Ser. A* **207**, (1951) 301.
25. Politano H. and Pouquet A., *Phys. Rev. E*, **57** (1998) R21.
26. Pisarenko D., Biferale L., Courvoisier D., Frisch U. and Vergassola M., *Phys. Fluids A*, **5** (1993) 2533.
27. Frisch U., *Turbulence: the Legacy of A. N. Kolmogorov* (Cambridge University Press) 1995.
28. L'vov V. S., Podivilov E., Pomyalov A., Procaccia I. and Vandembroucq D., *Phys. Rev. E*, **58** (1998) 1811.
29. Boffetta G., Carbone V., Giuliani P. and Veltri P., in preparation.
30. Basu A., Sain A., Dhar S. K. and Pandit R., *Phys. Rev. Lett.*, **81** (1998) 2687.
31. Benzi R., Ciliberto S., Tripicciono R., Baudet C., Massaioli F. and Succi S., *Phys. Rev. E*, **48** (1993) R29.
32. Brandenburg A., Enqvist K. and Olesen P., *Phys. Lett. B*, **392** (1997) 395
33. Boffetta G., Carbone V., Giuliani P., Veltri P., and Vulpiani A., *Phys. Rev. Lett.*, **83** (1999) 4662.